Performance analysis of optical vector analyzer based on optical single-sideband modulation

Min Xue, Yongjiu Zhao, Xiaowen Gu, and Shilong Pan*

Microwave Photonics Research Laboratory, College of Electronic and Information Engineering, Nanjing University of Aeronautics and Astronautics, Nanjing 210016, China
**Corresponding author: pans@ieee.org*

Received October 9, 2012; revised January 27, 2013; accepted February 4, 2013;
posted February 13, 2013 (Doc. ID 177723); published March 14, 2013

Optical vector network analyzers (OVNAs) based on optical single-sideband (OSSB) modulation are of great interest thanks to the potentially high measurement resolution. However, the measurement accuracy of the OSSB-based OVNA is limited by the high-order sidebands in the OSSB signal. To study the influence of the high-order optical sidebands in OSSB signals on the measurement accuracy, an analytical model is established to present the expression of the measurement error and a numerical simulation is performed. For the OSSB-based OVNA implemented by a 90-deg electrical hybrid coupler and a dual-drive modulator, when the −1st order sideband is fully suppressed by the OSSB modulation, the existence of the +2nd-order sideband severely degrades the resolution of the measurement, while the −3rd and −2nd order sidebands place a restriction on the dynamic range of the measurement. In addition, these sidebands also introduce evident measurement errors to the phase response. The study may provide a good guidance in designing the high performance OVNA.

OCIS codes: 130.4110, 190.4360, 120.5050, 060.2300, 350.4010.

1. INTRODUCTION

The rapid development of photonic systems demands high resolution and accurate measurement of the optical devices. The phase and magnitude responses are essential to obtain many key parameters for a device under test (DUT), such as the insertion loss, dispersion, group delay, polarization mode dispersion (PMD), polarization-dependent loss (PDL), and impulse response. Several methods were proposed to measure the phase and magnitude responses, such as the modulation phase-shift approach [1], the interferometry approach [2], and the optical single-sideband (OSSB) modulation-based optical vector network analyzer (OVNA) [3–8]. Among them, the measurement resolution of the OSSB-based OVNA can reach 78 kHz in experiment [8] and several hertz in theory [3]. In addition, the OSSB-based OVNA can measure polarization parameters, such as PMD, PDL, and so on, by simply incorporating a polarization beam splitter [5].

In the OSSB-based OVNA, the key component is the wideband OSSB modulator. Numerous techniques to generate the wideband OSSB signals were reported [9–14], such as the approaches based on a dual-drive Mach–Zehnder modulator (MZM) [9], an equivalent phase-shift fiber Bragg grating (PS-FBG) followed by a uniform FBG [10,11], an EAM-loop [12], an optical Hilbert transformer [13] or a steep-edge optical bandpass filter [8]. In the OSSB-based OVNA, the responses of the DUT are probed by one of the first-order sidebands, so it is highly desirable that the OSSB signal consist of the carrier and one of the first-order sidebands only. However, all the OSSB modulators generate considerable high-order sidebands if the phase modulation index of the modulator is large, which would significantly distort the measurement results. In [4], Hernández *et al.* pointed out that higher suppression of the residual sidebands in the generated OSSB signal would results in higher measurement accuracy, but a comprehensive study on the influence of the high-order sidebands on the measurement accuracy is still lacking.

In this paper, a theoretical and numerical investigation on the influence of the high-order sidebands on the measurement accuracy of the OSSB-based OVNA is performed. An analytical model is established for the OSSB-based OVNA implemented by a 90-deg electrical hybrid coupler and a dual-drive modulator, from which the expression of the measurement errors is deduced. Given that the −1st order sideband is fully suppressed by the OSSB modulation, analytical results show that the components beat by the +1st and +2nd order sidebands and the −3rd and −2nd order sidebands introduce considerable measurement errors. These results are confirmed by the numerical simulation in which an ultra-narrow-band PS-FBG is served as the DUT. The existence of the +2nd order sideband severely degrades the accuracy of the OSSB-based OVNA, while the −3rd and −2nd order sidebands place a restriction on the dynamic range of measurement. In addition, these sidebands also introduce evident measurement errors to the phase response. The analysis in the work can be extended to study other OSSB-based OVNAs.

2. ANALYTICAL ANALYSIS

Figure 1 shows a typical configuration of the OSSB-based OVNA. An optical carrier from a laser diode (LD) is modulated by a RF signal from a tunable RF source at an OSSB modulator. The OSSB modulator is composed of a 90-deg electrical hybrid coupler and a dual-drive MZM. Then, the OSSB signal propagates through a DUT. The DUT changes the phase and magnitude of each sideband in the OSSB signal. A photodetector (PD) is followed to convert the OSSB signal back to a RF signal. The phase and magnitude of the generated RF signal

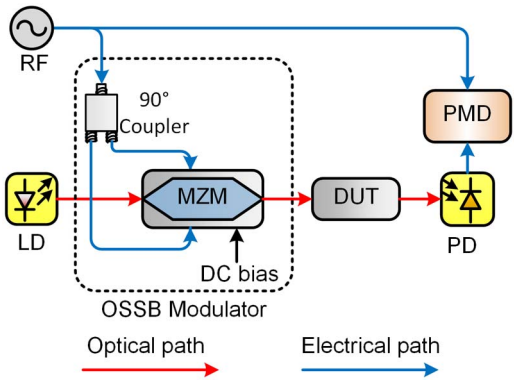

Fig. 1. (Color online) Schematic diagram of the OSSB-based OVNA. LD, laser diode; RF, radio frequency; MZM, Mach–Zehnder modulator; DUT, device under test; PD, photodetector, PMD, phase-magnitude detector.

are detected by a phase-magnitude detector. By scanning the frequency of the RF signal, the phase and magnitude responses of the DUT can be obtained.

Mathematically, the OSSB signal generated by the dual-drive MZM can be written as

$$E_{\mathrm{SSB}}^{\mathrm{in}}(t) = \exp(i\omega_o t)\left\{\exp\left[i\left(\beta\cos\omega_e t - \frac{\pi}{2}\right)\right] + \exp(i\beta\sin\omega_e t)\right\}, \quad (1)$$

where ω_o, ω_e are the angular frequency of the optical carrier and the RF signal, respectively, $\beta = \pi V/V\pi$ is the phase modulation index, V is the magnitude of the RF signal, and V_π is the half-wave voltage of the MZM. Based on the Jacobi–Anger expansion, the signal in Eq. (1) can be rewritten as

$$E_{\mathrm{SSB}}^{\mathrm{in}}(t) = \sum_{m=-\infty}^{\infty}\{J_m(\beta)(i^{m-1}+1)\exp[i(\omega_o + m\omega_e)t]\}, \quad (2)$$

where $J_m(\beta)$ is the mth order Bessel function of the first kind. The Fourier transform of the signal in (2) is

$$E_{\mathrm{SSB}}^{\mathrm{in}}(\omega) = \sum_{m=-\infty}^{\infty}\{2\pi J_m(\beta)(i^{m-1}+1) * \delta[\omega - (\omega_o + m\omega_e)]\}. \quad (3)$$

In the DUT, the phase and magnitude of the carrier and each sideband in the OSSB signal would be changed according to the transmission response of the DUT. After the DUT, the optical signal can be expressed by

$$\begin{aligned} E_{\mathrm{SSB}}^{\mathrm{out}}(\omega) &= E_{\mathrm{SSB}}^{\mathrm{in}}(\omega)\cdot H(\omega) \\ &= \sum_{m=-\infty}^{\infty}\{2\pi H(\omega_o + m\omega_e)J_m(\beta)(i^{m-1}+1) \\ &\quad * \delta[\omega - (\omega_o + m\omega_e)]\}, \end{aligned} \quad (4)$$

where $H(\omega)$ is the transmission response of the DUT.

After the square-law detection in the PD, we obtain

$$i_{\mathrm{PD}}(t) = \eta E_{\mathrm{SSB}}^{\mathrm{out}}(t)\cdot E_{\mathrm{SSB}}^{\mathrm{out}*}(t), \quad (5)$$

where η is the responsivity of the PD and $E_{\mathrm{SSB}}^{\mathrm{out}}(t)$ is the reverse Fourier transform of $E_{\mathrm{SSB}}^{\mathrm{out}}(\omega)$, given by

$$E_{\mathrm{SSB}}^{\mathrm{out}}(t) = \sum_{m=-\infty}^{\infty}\{H(\omega_o + m\omega_e)J_m(\beta)(i^{m-1}+1) \times \exp[i(\omega_o + m\omega_e)t]\}. \quad (6)$$

In the OSSB-based OVNA, the phase-magnitude detector only responds to the component with the same frequency of the reference signal, i.e., ω_e, so we have

$$\begin{aligned} i_{\mathrm{PD},\omega_e}(t) &= \eta\sum_{m=-\infty}^{\infty}\{(i^m+1)(i^{m-1}+1)^* J_{m+1}(\beta)J_m(\beta) \\ &\quad \cdot H[\omega_o + (m+1)\omega_e]H^*(\omega_o + m\omega_e)\exp(i\omega_e t) \\ &\quad + (i^m+1)^*(i^{m-1}+1)J_{m+1}(\beta)J_m(\beta) \\ &\quad \cdot H^*[\omega_o + (m+1)\omega_e]H(\omega_o + m\omega_e)\exp(-i\omega_e t)\} \\ &= 2\eta\,\mathrm{Re}\left\{\sum_{m=-\infty}^{\infty}[(i^m+1)(i^{m-1}+1)^* J_{m+1}(\beta)J_m(\beta) \right. \\ &\quad \left. \times H[\omega_o + (m+1)\omega_e]H^*(\omega_o + m\omega_e)\exp(i\omega_e t)]\right\}. \end{aligned} \quad (7)$$

As can be seen from Eq. (7), the ω_e component in the received signal is produced by the beat note of the $(m \pm 1)$th and mth-order optical sidebands. To simplify the analysis, Eq. (7) can be represented in the complex exponential form [15],

$$\begin{aligned} i_{\mathrm{PD},\omega_e}(t) &= 2\eta\sum_{m=-\infty}^{\infty}\{(i^m+1)(i^{m-1}+1)^* J_{m+1}(\beta)J_m(\beta) \\ &\quad \times H[\omega_o + (m+1)\omega_e]H^*(\omega_o + m\omega_e)\exp(i\omega_e t)\}. \end{aligned} \quad (8)$$

From Eq. (8), it is very hard to obtain $H(\omega)$ from the electrical current of the PD because the current is the sum of $H(\omega)$ at different frequencies. To simplify the measurement, it is highly desirable that the signal in Eq. (2) contains the optical carrier and the +1st order optical sideband only. In that case, the electrical current in Eq. (8) can be rewritten as

$$\begin{aligned} i_{m=0}(t) &= 4\sqrt{2}\eta J_0(\beta)J_1(\beta)H(\omega_o + \omega_e)H^*(\omega_o) \\ &\quad \times \exp\left[i\left(\omega_e t + \frac{\pi}{4}\right)\right]. \end{aligned} \quad (9)$$

Based on Eq. (9), the transmission response of the DUT can be achieved, given by

$$H(\omega_o + \omega_e) = \frac{i_{m=0}(t)}{4\sqrt{2}\eta J_0(\beta)J_1(\beta)H^*(\omega_o)\exp\left[i\left(\omega_e t + \frac{\pi}{4}\right)\right]}. \quad (10)$$

In the actual measurement [3–8], we always assume that $i_{\mathrm{PD},\omega_e}(t)$ equals $i_{m=0}(t)$, which is the case that can only be obtained when $\beta \to 0$. When $\beta \neq 0$, the actual responses we obtained in the measurement should be

$$\begin{aligned} H_{\mathrm{measured}}(\omega_o + \omega_e) &= \frac{i_{m=0}(t)}{4\sqrt{2}\eta J_0(\beta)J_1(\beta)H^*(\omega_o)\exp\left[i\left(\omega_e t - \frac{\pi}{4}\right)\right]} + \Delta \\ &= H(\omega_o + \omega_e) + \Delta, \end{aligned} \quad (11)$$

where Δ is the deviation between the measured and actual responses introduced by the high-order sidebands in the OSSB signal, given by

$$\Delta = \frac{\sum_{\substack{m=-\infty \\ m\neq 0}}^{\infty}\{(i^m+1)(i^{m-1}+1)^* J_{m+1}(\beta)J_m(\beta)H[\omega_o+(m+1)\omega_e]H^*(\omega_o+m\omega_e)\}}{2\sqrt{2}J_0(\beta)J_1(\beta)H^*(\omega_o)\exp\left(i\frac{\pi}{4}\right)}. \tag{12}$$

As can be seen from Eq. (12), the measurement error is deeply dependent on the transmission characteristics of the DUT. To give an intuitive understanding of Eq. (12), we let the response of the DUT be $H(\omega)=1$. Thus, the measurement error is written as

$$\Delta = \frac{\sum_{\substack{m=-\infty \\ m\neq 0}}^{\infty}[(i^m+1)(i^{m-1}+1)^* J_{m+1}(\beta)J_m(\beta)]}{2\sqrt{2}J_0(\beta)J_1(\beta)\exp\left(i\frac{\pi}{4}\right)}. \tag{13}$$

In Eq. (13), each term in the right side represents the measurement error introduced by the beat component of the mth and $(m+1)$th-order sidebands. For practical measurement, the phase modulation index β is usually less than π, due to the limited microwave power applied to the MZM. For $0 \le \beta \le \pi$, the Bessel function J_n for $n \ge 4$ are all monotonically increasing with respect to β and monotonically decreasing with respect to the order of Bessel function n. Given that $J_3(\pi)=0.33346$, $J_4(\pi)=0.15142$, and $J_5(\pi)=0.05214$, it is reasonable to ignore the optical sidebands with order higher than 4 in our analysis. Thus, Eq. (13) can be simplified to

$$\Delta = \frac{J_{-3}(\beta)J_{-4}(\beta)}{J_0(\beta)J_1(\beta)} + \frac{J_{-2}(\beta)J_{-3}(\beta)}{J_0(\beta)J_1(\beta)} + \frac{J_2(\beta)J_1(\beta)}{J_0(\beta)J_1(\beta)}. \tag{14}$$

The three terms in the right side of Eq. (14) represent the measurement errors introduced by the components beat by the −4th and −3rd, −3rd and −2nd, and +1st and +2nd order sidebands, respectively. Because the −1st and +3rd-order sidebands are eliminated by the OSSB modulation, the components beat by the −2nd and −1st, +2nd and +3rd, and +3rd and −4th-order sidebands are not presented. Figure 2 shows the measurement error of the magnitude response introduced by each term. As can be seen, the larger the modulation index is, the bigger the measurement error will be. The biggest error is originated from the component beat by the +1st and +2nd order sidebands. At a phase modulation index of $\pi/3$, which is a practical value in the measurement, the error is greater than 16.7%, which could significantly distort the measured responses. Since we have assumed $H(\omega)=1$, the phase of the component beat by the mth and $(m+1)$th order sidebands always equals to $\pi/4$. As a result, in Eq. (13) we cannot find the errors in phase. To reveal the errors of the phase measurement, a complex $H(\omega)$ must be assumed, which is too complicated for the analytical analysis. Therefore, numerical simulations are performed in the next section.

It should be noted that although lower modulation index would produce smaller measurement error, it would reduce the measurement dynamic range because the power level of the signal after detection is very low. For example, Fig. 3 shows a typical curve of the measurement dynamic range as a function of the modulation index. To achieve Fig. 3, the power of the optical signal to the PD is assumed to be 10 dBm, the responsivity of the PD is 0.8 A/W, and the noise floor of the system is −90 dBm. As can be seen, the largest dynamic range is 60.71 dB at a modulation index of 1.082. If the modulation index is smaller than 0.22, the measurement dynamic range is less than 50.71, 10 dB lower than the maximum.

3. NUMERICAL SIMULATION

In order to further investigate the influence of the high-order sidebands in the OSSB signal on the measurement accuracy of the OSSB-based OVNA, numerical simulation of the OSSB-based OVNA is performed. In the simulation, the DUT is assumed to be an ideal PS-FBG with the phase and magnitude responses shown in Fig. 4. The PS-FBG has a center wavelength of 1550 nm, a notch depth of 59.46 dB, a 3 dB bandwidth of 11.1 GHz, and a phase-shift of 180°. Here, the center frequency is defined as the average of the two frequencies at which the transmittance is 15 dB lower than the transmission peak; the notch depth is defined as the absolute value of the difference between the maximum and minimum transmittances; the 3 dB bandwidth is defined as the absolute value of the difference between the two frequencies at which the

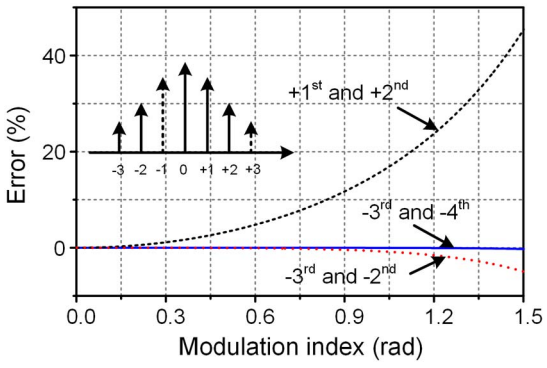

Fig. 2. (Color online) Errors introduced by the components beat by the mth and $(m+1)$th order sidebands.

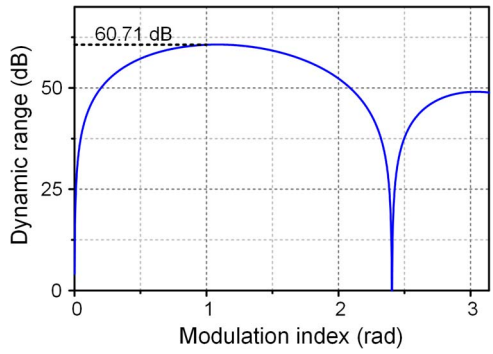

Fig. 3. (Color online) Typical curve of the measurement dynamic range as a function of the modulation index.

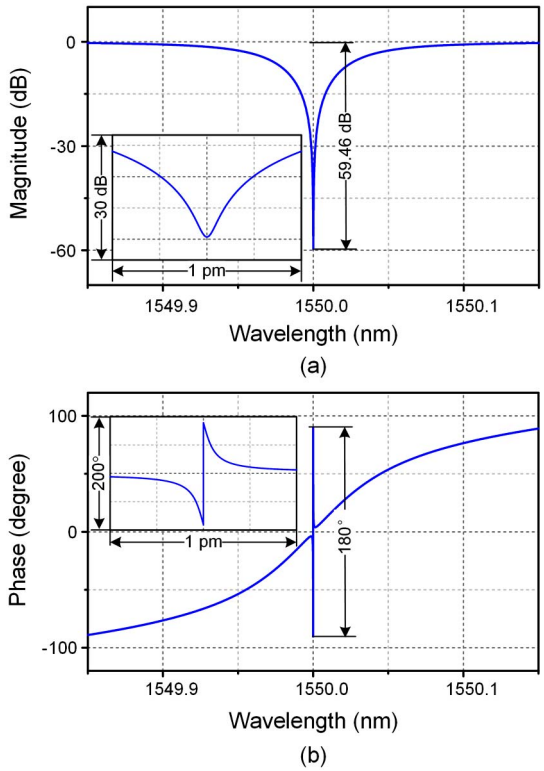

Fig. 4. (Color online) Actual responses of the PS-FBG. (a) The magnitude response and (b) the phase response.

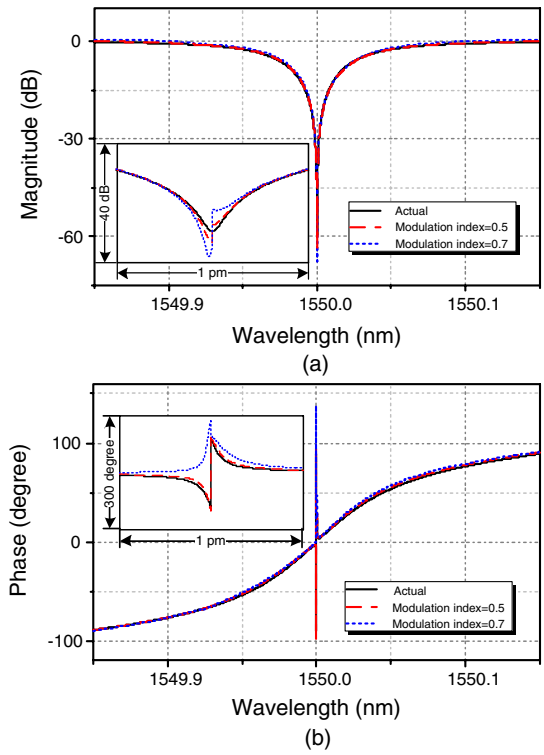

Fig. 5. (Color online) Simulated measurement of the PS-FBG when the phase modulation indices are 0.5 and 0.7, respectively. (a) The magnitude response and (b) the phase response.

transmittance is 3 dB lower than the transmission peak; and the phase-shift is defined as the absolute value of the difference between the maximum and minimum phases around the center wavelength. Other parameters used in the simulation are as follows. The center wavelength of the LD is 50 kHz; the RF source has a scanning step of 50 kHz and a frequency range of 40 GHz; the bandwidth of the PD is 40 GHz. According to the analytical analysis above, only the −4th to +4th order sidebands are considered in the simulation.

Figure 5 shows the simulated magnitude and phase responses of the PS-FBG when the modulation indices are 0.5 and 0.7, respectively. The actual magnitude and phase responses of the PS-FBG are also plotted for reference. As can be seen, the OSSB-based OVNA can measure the actual responses when the modulation index is small. But when the modulation index is large, significant distortions in both magnitude and phase responses are observed, especially around the wavelength notch. According to the analytical analysis in the previous part, the distortion is introduced by the high-order sidebands in the OSSB signal, which are generated by the large-signal modulation in the OSSB modulator. From Eq. (12), the −4th, −3rd, −2nd, and +2nd order sidebands introduce appreciable measurement error. Therefore, to better understand the influence of each high-order sidebands, the influence of the −4th, −3rd, −2nd, and +2nd order sidebands on the notch depth, center frequency, 3 dB bandwidth, and phase shift is numerically studied.

A. Magnitude Response

Figure 6(a) shows the simulated notch depth as a function of the modulation index when one of the undesired sidebands is removed. Since the +1st order sideband is largely attenuated by the PS-FBG in the notch center (for example, 59.46 dB in the simulation), the beat note between the −2nd and −3rd order sidebands contributes a considerable portion to the power of the generated ω_e component. Therefore, the notch depth should be greatly affected by the −2nd and −3rd order sidebands. As can be seen from Fig. 6(a), if both of the −2nd and −3rd order sidebands present in the OSSB signal, there is large measurement error of the notch depth at $\beta \geq 0.4$. According to Eq. (12), the beat note between the −2nd and −3rd order sidebands and that between the +1st order sideband and the optical carrier are out of phase. Thus, with the increase of the modulation index, the total power of the ω_e component firstly decreases because the power of the high-order sidebands increases faster than that of the first-order sideband, and then increases since the power of the beat note between the −2nd and −3rd order sidebands is greater than that between the +1st order sideband and the optical carrier. This results in the increasing/decreasing notch depth before/after 0.65, as shown in Fig. 6(a). Because the accurate identification of the notch depth is very important for an OVNA with large dynamic range, it would be highly desirable to remove −2nd or −3rd order sideband in the OSSB signal to increase the dynamic range of the OSSB-based OVNA.

Figure 6(b) shows the measurement error of the center frequency introduced by the −4th, −3rd, −2nd, and +2nd order sidebands, respectively. When both of the +1st and +2nd order sidebands are located in the left edge of the PS-FBG, they would undergo increasing attenuation in the PS-FBG as the frequency of the RF signal increases, while the −3rd and −2nd order sidebands are almost unaffected. Because the beat note between the −2nd and −3rd order sidebands and that between the +1st order sideband and the optical carrier are out

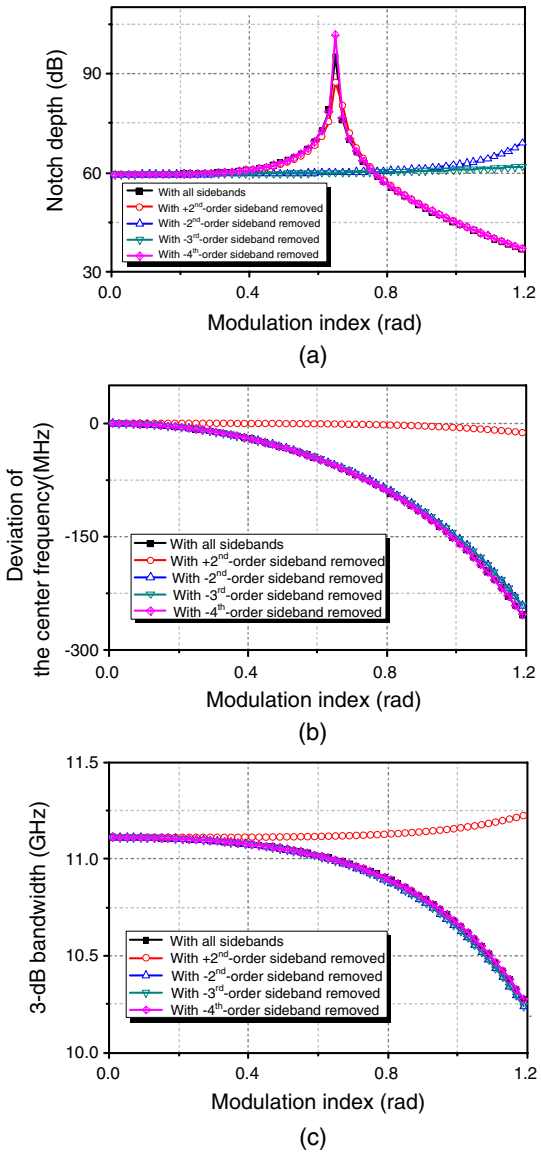

Fig. 6. (Color online) Influence of the −4th, −3rd, −2nd, and +2nd order sidebands on (a) the notch depth, (b) center frequency, and (c) 3 dB bandwidth.

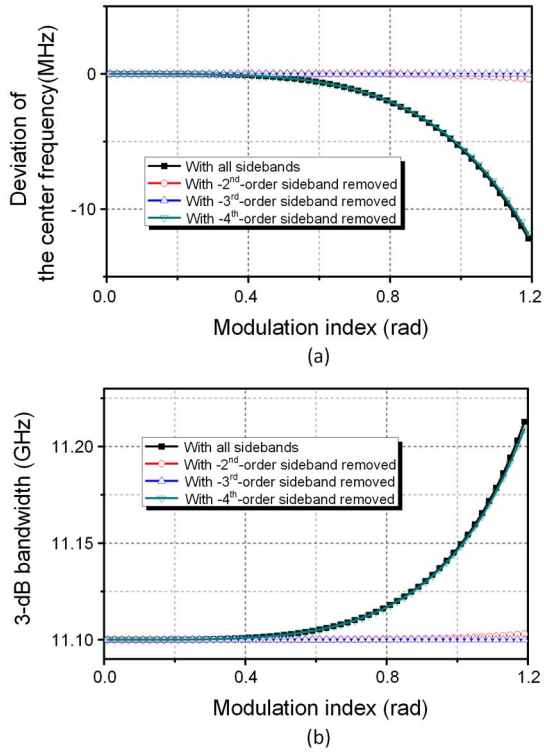

Fig. 7. (Color online) Influence of the −4th, −3rd, and −2nd order sidebands on (a) the center frequency and (b) the 3 dB bandwidth with the +2nd order sideband removed.

of phase, the measured frequency response would decrease faster than the actual one. When the +2nd order sideband is located at the right edge of the PS-FBG, its attenuation would decrease as the frequency of the RF signal increases. According to Eq. (12), the beat note between the +2nd and +1st order sidebands and that between the +1st order sideband and the optical carrier are in phase, so decreasing of the measured frequency response would be finally stopped by the +2nd order sideband, resulting a notch with a center frequency smaller than the actual one, as shown in Fig. 6(b) and also in the inset of Fig. 5(a). The center frequency shift can be as large as hundreds of MHz, which greatly degrades the wavelength resolution of the OSSB-based OVNA. This situation can be improved if the +2nd order sideband is removed. In that case, the center frequency shift is 2 MHz at a phase modulation index of 0.8.

Similarly, the +2nd order sideband would also introduce large measurement error to the 3 dB bandwidth. Figure 6(c) shows the 3 dB bandwidth versus the modulation index. With all sidebands considered, the 3 dB bandwidth is generally smaller than the actual value (11.1 GHz). At a phase modulation index of 0.8, the deviation is about 0.2 GHz. If the +2nd order sideband is removed, the error for the 3 dB bandwidth is only 17.06 MHz at a phase modulation index of 0.8.

Since the +2nd order sideband greatly degrades the resolution of the measurement, it should be removed for a high-performance, OSSB-based OVNA. Therefore, the measurement error induced by −4th, −3rd, and −2nd order sidebands without the +2nd order sideband becomes interesting. Figure 7 shows the deviation of the center frequency and the 3 dB bandwidth as a function of the modulation index when the +2nd order sideband is removed. As can be seen from Figs. 7(a) and 7(b), the resolution of the OSSB-based OVNA can be further improved if the −2nd or −3rd order sideband in the OSSB signal is also removed. For example, if both +2nd and −2nd order sidebands are removed, the center frequency shift is only 28.3 kHz, and the error for the 3 dB bandwidth is only 0.22 MHz at a phase modulation index of 0.8.

B. Phase Response

Figure 8 shows the simulated phase-shift of the PS-FBG as a function of the modulation index when one of the undesired sidebands is removed. Since the phase-shift of the PS-FBG is evaluated around the center of the notch where the +1st-order sideband is largely attenuated (59.46 dB in the simulation), the beat note between the −2nd and −3rd order sidebands contributes a considerable portion to the power of the generated ω_e component. Therefore, the phase-shift should be also greatly affected by the −2nd and −3rd order sidebands. As can be seen from Fig. 8, if both of the −2nd and −3rd order

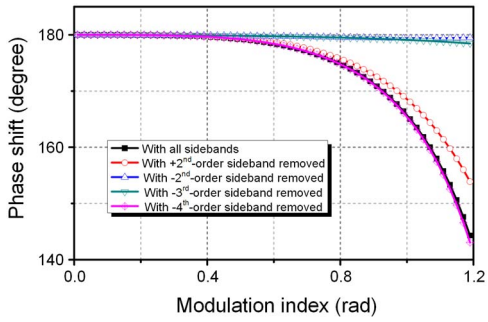

Fig. 8. (Color online) Influence of the −4th, −3rd, −2nd, and +2nd order sidebands on the measured phase-shift of the PS-FBG.

sidebands present in the OSSB signal, there is large measurement error of the phase-shift. The −4th order sideband almost has no influence on the simulated phase-shift of the PS-FBG because of its very low power. Although the +1st order sideband is largely attenuated when measuring the phase-shift, the beat note between the +1st and +2nd order sidebands still introduces the some measurement error because the power of the +2nd-order sideband is relatively large. Thus, in order to obtain the accurate phase response of the DUT, such as the PS-FBG, the −2nd or −3rd order sideband as well as the +2nd order sideband should be removed.

4. CONCLUSIONS

A theoretical and numerical investigation on the influence of the high-order sidebands in the OSSB signal on the measurement accuracy of the OSSB-based OVNA was performed. Analytical results show that the components beat by the +1st and +2nd order sidebands and the −3rd and −2nd order sidebands introduce considerable measurement errors in the magnitude and phase responses measurement. These results agree well with the numerical simulation in which an ultra-narrowband PS-FBG is served as the DUT. To improve the resolution of the OSSB-based OVNA, the +2nd order sideband should be largely suppressed, while to enlarge the dynamic range of measurement one of the −3rd and −2nd order sidebands should be removed. In addition, these sidebands also introduce large measurement errors to the measured phase response.

ACKNOWLEDGMENTS

This work was supported in part by the National Natural Science Foundation of China (61107063), the National Basic Research Program of China (2012CB315705), the Aviation Science Foundation of China (2012ZD52052), the Jiangshu Provincial Funds for Distinguished Young Scientists (BK2012031), the Jiangsu Provincial Program for High-level Talents in Six Areas (DZXX-034), the Fundamental Research Funds for the Central Universities (NE2012002), and a Project Funded by the Priority Academic Program Development of Jiangsu Higher Education Institutions.

REFERENCES

1. T. Niemi, M. Uusimaa, and H. Ludvigsen, "Limitations of phase-shift method in measuring dense group delay ripple of fiber Bragg gratings," IEEE Photon. Technol. Lett. **13**, 1334–1336 (2001).
2. G. D. VanWiggeren, A. R. Motamedi, and D. M. Baney, "Single-scan interferometric component analyzer," IEEE Photon. Technol. Lett. **15**, 263–265 (2003).
3. J. E. Román, M. Y. Frankel, and R. D. Esman, "Spectral characterization of fiber gratings with high resolution," Opt. Lett. **23**, 939–941 (1998).
4. R. Hernandez, A. Loayssa, and D. Benito, "Optical vector network analysis based on single-sideband modulation," Opt. Eng. **43**, 2418–2421 (2004).
5. M. Sagues, M. Perez, and A. Loayssa, "Measurement of polarization dependent loss, polarization mode dispersion and group delay of optical components using swept optical single sideband modulated signals," Opt. Express **16**, 16181–16188 (2008).
6. M. Sagues and A. Loayssa, "Spectral characterisation of polarisation dependent loss of optical components using optical single sideband modulation," Electron. Lett. **47**, 47–48 (2011).
7. M. Sagues and A. Loayssa, "Swept optical single sideband modulation for spectral measurement applications using stimulated Brillouin scattering," Opt. Express **18**, 17555–17568 (2010).
8. Z. Z. Tang, S. L. Pan, and J. P. Yao, "A high resolution optical vector network analyzer based on a wideband and wavelength-tunable optical single-sideband modulator," Opt. Express **20**, 6555–6560 (2012).
9. G. H. Smith, D. Novak, and Z. Ahmed, "Overcoming chromatic-dispersion effects in fiber-wireless systems incorporating external modulators," IEEE Trans. Microwave Theory Tech. **45**, 1410–1415 (1997).
10. J. Park, W. V. Sorin, and K. Y. Lau, "Elimination of the fibre chromatic dispersion penalty on 1550 nm millimetre-wave optical transmission," Electron. Lett. **33**, 512–513 (1997).
11. S. R. Blais and J. P. Yao, "Optical single sideband modulation using an ultranarrow dual-transmission-band fiber Bragg grating," IEEE Photon. Technol. Lett. **18**, 2230–2232 (2006).
12. G. Ning, J. Q. Zhou, L. Cheng, S. Aditya, and P. Shum, "Generation of different modulation formats using Sagnac fiber loop with one electroabsorption modulator," IEEE Photon. Technol. Lett. **20**, 297–299 (2008).
13. Z. Li, H. Chi, X. M. Zhang, and J. P. Yao, "Optical single-sideband modulation using a fiber-Bragg-grating-based optical Hilbert transformer," IEEE Photon. Technol. Lett. **23**, 558–560 (2011).
14. A. Villafranca, J. A. Lazaro, I. Salinas, and I. Garces, "Stimulated Brillouin scattering gain profile characterization by interaction between two narrow-linewidth optical sources," Opt. Express **13**, 7336–7341 (2005).
15. A. V. Oppenheim, A. S. Willsky, and S. H. Nawab, *Signals and Systems*, 2nd ed. (Prentice-Hall, 1997).